Gating of Single Non-*Shaker* A-Type Potassium Channels in Larval *Drosophila* Neurons

CHARLES K. SOLC and RICHARD W. ALDRICH

From the Department of Neurobiology, Stanford University School of Medicine, Stanford, California 94305-5401.

ABSTRACT The voltage-dependent gating of transient A_2-type potassium channels from primary cultures of larval *Drosophila* central nervous system neurons was studied using whole-cell and single-channel voltage clamp. A_2 channels are genetically distinct from the *Shaker* A_1 channels observed in *Drosophila* muscle, and differ in single-channel conductance, voltage dependence, and gating kinetics. Single A_2 channels were recorded and analyzed at -30, -10, $+10$, and $+30$ mV. The channels opened in bursts in response to depolarizing steps, with three to four openings per burst and two to three bursts per 480-ms pulse (2.8-ms burst criterion). Mean open durations were in a range of 2–4 ms and mean burst durations in a range of 9–17 ms. With the exception of the first latency distributions, none of the means of the distributions measured showed a consistent trend with voltage. Macroscopic inactivation of both whole-cell A currents and ensemble average currents of single A_2 channels was well fitted by a sum of two exponentials. The fast time constants in different cells were in a range of 9–25 ms, and the slow time constants in a range of 60–140 ms. A six-state kinetic model (three closed, one open, two inactivated states) was tested at four command voltages by fitting frequency histograms of open durations, burst durations, burst closed durations, number of openings per burst, and number of bursts per trace. The model provided good fits to these data, as well as to the ensemble averages. With the exception of the rates leading to initial opening, the transitions in the model were largely independent of voltage.

INTRODUCTION

Most neurons contain several kinetically distinguishable types of voltage-activated potassium channels (see reviews by Latorre et al., 1984; Rudy, 1988). Differences in the voltage dependence and gating kinetics of these channels help determine the cell's firing properties (see reviews by Adams et al., 1980; Adams and Galvan, 1986; Thompson and Aldrich, 1980). In order to understand better the basic mechanisms

Dr. Charles K. Solc's present address is Department of Neurology, Wellman 414, Howard Hughes Medical Institute and Massachusetts General Hospital, Boston, MA 02114.
Address reprint requests to Dr. Richard W. Aldrich, Department of Neurobiology, Stanford University School of Medicine, Stanford, CA 94305-5401.

J. GEN. PHYSIOL. © The Rockefeller University Press · 0022-1295/90/07/0135/31 $2.00
Volume 96 July 1990 135–165

that underlie voltage-dependent gating, it is desirable to combine both biophysical and molecular approaches in the study of ion channels. *Drosophila* is an ideal organism for such an integrated approach, as has been demonstrated by the recent cloning and analysis of the *Shaker* locus (Baumann et al., 1987; Papazian et al., 1987; Tempel et al., 1987; Kamb et al., 1987, 1988; Iverson et al., 1988; Pongs et al., 1988; Schwarz et al., 1988; Timpe et al., 1988*a*, *b*; Zagotta et al. 1989) In this article, we present an analysis of the gating properties of a voltage-dependent transient potassium channel (termed the A_2 channel) that is distinct from *Shaker* channels and is found in the somata of cultured larval central nervous system (CNS) *Drosophila* neurons.

Transient potassium current was first documented by Hagiwara et al. (1961), and characterized by Connor and Stevens (1971*a*) and Neher (1971). Connor and Stevens (1971*a*) termed the transient current in *Anidosoris* neurons A current. The A current was observed during depolarizations positive to −50 mV after a hyperpolarizing prepulse to remove resting inactivation. The midpoint of the resting inactivation curve was ~75 mV. The inactivation time course was independent of voltage, and was well fitted by single-exponential function with time constants between 220 and 600 ms (5°C, $Q_{10} = \sim 3$). A quantitative model of the voltage response of *Anidosoris* neurons to current injection suggested that the A current was primarily responsible for controlling the interspike interval (Connor and Stevens, 1971*b*).

Potassium currents similar to the A current, subsequently described in many cell types (see reviews by Adams and Galvan, 1987; Rudy, 1988; Thompson and Aldrich, 1980), were first observed in *Drosophila* under voltage clamp by Salkoff and Wyman (1981*a*). The currents, recorded in pupal flight muscle, were eliminated in flies homozygous for mutations at the *Shaker* locus (Salkoff and Wyman, 1981*b*). Several studies suggested that potassium channels affected by *Shaker* play a role in the repolarization of the action potential in axons and nerve terminals (Jan et al., 1977; Tanouye et al., 1981; Ganetzky and Wu, 1983), indicating that the *Shaker* product is likely to be present in neurons as well as muscle. The ionic currents in neurons, however, were not studied with voltage clamp. More recently, patch-clamp studies of larval *Drosophila* CNS neurons in primary culture (Wu et al., 1983; Ganetzky and Wu, 1985; Solc et al., 1987; Solc and Aldrich, 1988) revealed several types of K channels, distinguished at the single-channel level. Among these was a transient A-type channel (termed A_2) that was distinct from the A-type potassium channels in *Drosophila* muscle (termed A_1), based on single-channel conductance, voltage dependence, gating kinetics, and on the lack of an effect of the Sh^{KS133} mutation on A_2 channel expression (Solc et al., 1987). Whereas the macroscopic gating properties of A_1 channels from embryonic myotubes (Solc et al., 1987; Zagotta et al., 1988) are similar to the A-type currents initially observed in *Drosophila* pupal muscle (Salkoff and Wyman, 1981*a*), the macroscopic gating properties of A_2 channels are similar to the A current described by Connor and Stevens (1971*A*). A_2 channels begin to activate at lower voltages, have a more negative midpoint of prepulse inactivation, and inactivate more slowly than A_1 channels (Solc et al., 1987). Furthermore, the macroscopic inactivation time course of A_2 channels is not voltage dependent, whereas that of A_1 channels is.

In this paper we analyze the gating of the A_2 channels in detail at the whole-cell and single-channel levels, and propose a kinetic model that accounts for the

observed gating properties. In addition, we provide further evidence that the gene(s) coding for A_2 channels are independent of the *Shaker* locus.

METHODS

Fly Stocks

The experiments were done using cells from either Canton S wild type or a fused synthetic deficiency stock of *Drosophila* missing most of the *Shaker* coding region. The deficiency stock, generously provided by Dr. T. Schwarz, was generated by an X-ray-induced fusion of the proximal segment of T(x;y)W32 and the distal segment of T(x;y)B55. The stocks were maintained on cornmeal-yeast-dextrose medium in an incubator at 22°C.

Cell Culture

Neuronal cultures were prepared as described previously (Solc and Aldrich, 1988; Wu et al., 1983): 10–15 late third instar larvae were collected and washed in 70% ethanol for 1–2 min. Brain and ventral ganglion complexes were dissected in phosphate-buffered saline (PBS), mechanically teased to rupture the neurolemma, and incubated for 45–75 min in a calcium-free magnesium-free PBS solution containing 0.5 mg/ml collagenase (type I, Sigma Chemical Co., St. Louis, MO). The preparation was centrifuged for 1–2 min at 3,000–4,000 rpm and the supernatant was discarded. The pellet was resuspended in modified Schneider's medium (Gibco Laboratories, Grand Island, NY) supplemented with 1.5% penicillin/streptomycin and 10 or 20% fetal calf serum (Gibco Laboratories or Hazelton Systems, Lenexa, KS), the cells were triturated until clumps of tissue were no longer visible, and plated on 12-mm round coverslips at a density of one-half to one brain/ganglion complex per coverslip. An extra coverslip was often placed on top of the cells, as this was found to improve viability. Cultures were maintained in 35-mm dishes with 1.5–2 ml of medium at 20–22°C for 3–10 d before voltage clamp experiments were conducted.

Electrophysiology

Cells ranging from 5 to 12 μm in diameter were voltage-clamped using the whole-cell and outside-out patch recording methods (Hamill et al., 1981). The electrodes had resistances of 2–12 MΩ when filled with the standard solutions described below. The pipette potential was nulled immediately before obtaining a tight seal on the cell. The voltages given in this study were not corrected for the junction potential, which was estimated to be <5 mV from the reversal potentials measured for potassium channels in symmetrical potassium solutions. Whole-cell input resistances were typically between 10 and 30 GΩ. Data were recorded with a model EPC-7 (List Medical/Medical Systems, Greenvale, NY) or Axopatch (Axon Instruments, Inc., Foster City, CA) patch clamp amplifier. Whole-cell linear leakage and uncompensated capacity currents were subtracted using a scaled average of currents elicited by 16–32 20-mV depolarizations from the holding potential. Series resistance compensation was not routinely used, because all of the whole-cell A currents considered in this study were <1 nA at +40 mV. Assuming a series resistance of 10 MΩ, approximately three times the resistance of a typical whole-cell electrode, a 1-nA current would produce a series resistance error of 10 mV. Since the time course of decay of A_2 currents (the only macroscopic kinetic property measured in this study) is essentially independent of voltage (see Fig. 3), even a 10-mV error would be insignificant. The currents were low-pass filtered with an eight-pole Bessel filter (Frequency Devices, Inc., Haverhill, MA), digitized at frequencies indicated in the figure legends, and stored for later analysis on a Digital Equipment Corporation 11/73 computer (Indec Systems, Sunnyvale, CA).

The ionic composition of the standard bath solution was (in millimolar): 140 NaCl, 2 KCl, 4 $MgCl_2$, 2 $CaCl_2$, 5 HEPES (NaOH), pH 7.1–7.2. The internal solution contained (in millimolar): 70 KF, 70 KCl, 2 $MgCl_2$, 11 EGTA, 1 $CaCl_2$, 10 HEPES (KOH), pH 7.1–7.2. The calculated internal free calcium concentration was ~10 nM. All experiments were conducted at room temperature (19–23°C).

Single-Channel Analysis

All patches used for quantitative analysis contained only one channel. The number of active channels in a patch was determined by observing the maximum number of simultaneously open channels at strongly depolarized voltages. This method provides an accurate estimate if the open probability [$P(O)$] of individual channels is relatively high and if a sufficient number of records are inspected. Since the peak $P(O)$ of A_2 channels is 0.4–0.6, and all runs used for analysis had at least 64 records, the probability of not seeing two channels if two were present in the patch is exceedingly small. Data from multichannel patches were in qualitative agreement with data from single-channel patches. Leakage and uncompensated capacity currents were digitally subtracted using leak templates constructed by fitting smooth functions to records with no openings. Single-channel amplitude was determined from amplitude histograms of traces with a high $P(O)$. The current records were then idealized using a 50% amplitude criterion to detect opening and closing transitions (Colquhoun and Sigworth, 1983). Duration histograms were generated from the idealized data. We did not correct for missed events (unresolved openings and closures), and address some possible consequences of this in the discussion. Ensemble averages were generated from the idealized data. Ensemble averages were expressed in probability units, determined by dividing the current averages (in units of picoamperes) by the number of channels in the patch (one) and by the unitary current amplitude.

RESULTS

Gating of Whole-Cell A Current

Several kinetically distinct types of voltage-dependent potassium channels can be recorded from cultured larval *Drosophila* neurons (Solc and Aldrich, 1988). A subset of the cells express primarily the A-type current with little detectable contribution from the other channel types. Whole-cell currents from a cell of this type are shown in Fig. 1. A family of currents recorded in response to 450-ms depolarizing voltage steps between −50 and +40 mV is shown in Fig. 1 *A*. The currents, which become evident between −45 and −40 mV, peak 3–6 ms after the onset of the depolarizing voltage pulse and inactivate. A current activation is shown on a faster time scale in Fig. 1 *C*. The currents turn on more rapidly at higher voltages. Fig. 1 *B* shows a family of currents recorded at +20 mV after prepulses to voltages between −100 and −40 mV. Prepulses to −40 mV inactivated over 95% of the current. The peak current–voltage relation of the currents in Fig. 1 *A* and the prepulse inactivation curve of the currents in Fig. 1 *B* are shown in Fig. 1 *D*. The prepulse inactivation data are fitted with an equation derived from the Boltzmann distribution, which describes the fraction of channels available to open:

$$\frac{I}{I_0} = \frac{1}{1 + e\left(\frac{V + V_m}{S}\right)}, \tag{1}$$

where Vm = 73 mV and IS = 6.9. Means ± SD for 23 cells were Vm = 75.1 ± 6.0 mV and S = 7.3 ± 1.2.

The macroscopic inactivation time course of the whole-cell A current varied somewhat from cell to cell. Time to half-inactivation ranged from 20 to 150 ms. The more rapidly inactivating currents are likely due to A_2 channels since the whole-cell

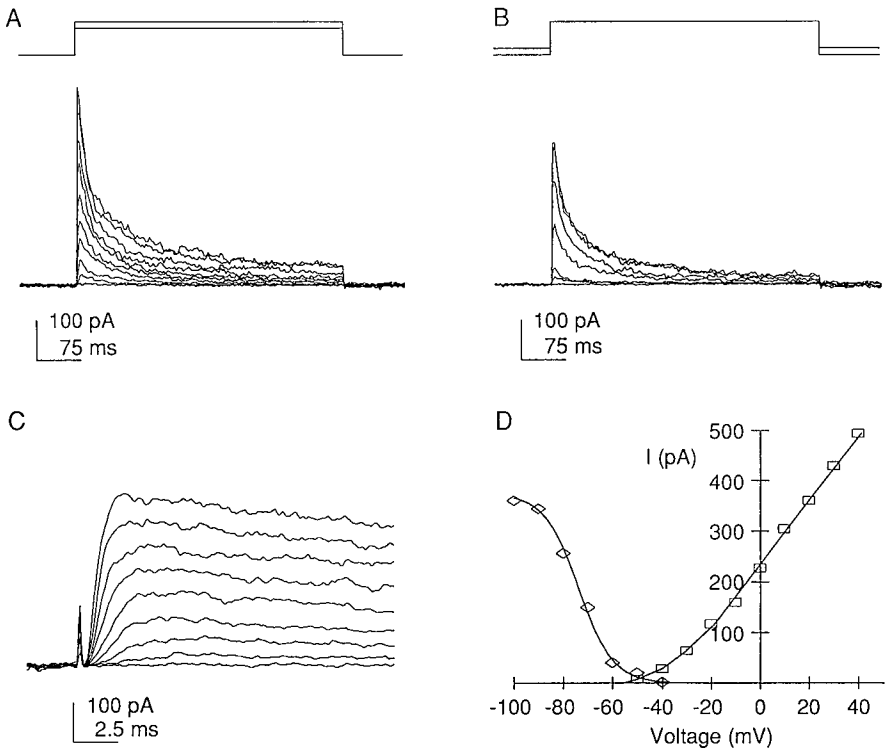

FIGURE 1. Families and current-voltage relation of whole-cell A currents in *Drosophila* neurons. (*A*) Whole-cell A currents in response to depolarizing voltage steps, applied at 3-s intervals, from a prepulse voltage of −90 mV. The step voltage was varied between −40 and +50 mV in 10-mV increments. Prepulse duration was 300 ms. (*B*) Whole-cell A currents elicited by steps to +20 mV from a range of prepulse voltages (−100 to −40 mV in 10-mV increments). Prepulse duration was 300 ms. Same cell as in *A*. (*C*) Whole-cell A currents recorded during 15-ms steps to voltages between −50 and +30 from a prepulse voltage of −100 mV. (*D*) Peak current–voltage relations of currents in *A* plotted *vs.* command voltage and currents in *B* plotted *vs.* prepulse voltage. The data were filtered at 2 kHz and digitized at 3 ms per point (*A* and *B*) or 100 μs per point (*c*).

gating properties agree well with single-channel measurements, and since even the most rapidly inactivating currents were observed in cells deficient for the *Shaker* locus as well as in wild-type cells (Solc, 1989). More slowly inactivating currents in the whole-cell configuration are more difficult to interpret because of possible contamination by other channel types, such as K_d channels (Solc and Aldrich, 1988). In

outside-out patches from such cells, however, we have observed instances of A_2 channels with macroscopic kinetics indistinguishable from those illustrated in Fig. 1, as well as A_2 channels with slower macroscopic inactivation.

Macroscopic inactivation. A sum of two exponentials was generally required to fit the decay of the whole-cell current, though in some cases a single exponential was sufficient. Fig. 2 shows whole-cell A_2 currents recorded at voltages between -30 and $+40$ mV. The records were fitted with a sum of two exponentials plus a baseline using an unweighted least-squares optimization routine. Because the currents were recorded in the whole-cell configuration, it is possible that the nonexponential decay resulted from more than one class of channel decaying exponentially at different rates. While we cannot exclude this possibility for the data in Fig. 2, we know, based on single-channel evidence, that double-exponential decay is an inherent property of A_2 channel kinetics (Solc and Aldrich, 1988; see also below). The magnitude of the fast and slow time constants, and the fraction of the fast time constant at each voltage are shown in Fig. 3. The symbols represent parameters of fits to three individual records, and the lines represent the parameters of fits to the average of the three records at each voltage. Neither the magnitude nor the relative contributions of the fast and slow time constants were strongly voltage dependent in the voltage range between -30 and $+40$ mV. The values of the fast and slow time constants ranged in different cells between 9 and 25 ms, and 60 and 140 ms, respectively.

A double-exponential macroscopic inactivation time course is consistent with several kinetic schemes, including those with two open states, or with two inactivated states (Chiu, 1977; Sigworth, 1981). Single-channel recording can distinguish between these possibilities, and provide additional insights into the gating of the A_2 channels.

Gating of Single A_2 Channels

Single A_2 channels were recorded from 25 cell-free patches. Five of these were suitable for analysis because they contained one A_2 channel, did not contain other channel types, and remained stable long enough to gather the necessary data.

Two single-channel records are shown at each of four command voltages in Fig. 4. The channels open rapidly after the voltage step, reopen a few times (a burst) and close to a relatively long-lived closed state. The observation of bursts of openings suggests that there are at least two closed states with considerably different mean dwell times: a short-lifetime state corresponding to closed durations within the burst, and a long-lifetime state corresponding to closed durations between bursts (Nelson and Sachs, 1979; Patlak et al., 1979; Conti and Neher, 1980; Sakmann et al., 1980; Colquhoun and Hawkes, 1981). Inspection of closed duration distributions consistently revealed at least two well-separated components at all voltages. In situations where bursts can be clearly identified, the evaluation of certain kinetic schemes can be simplified by defining a burst with a burst criterion duration (Magleby and Pallotta, 1983). All closed intervals shorter than the criterion are defined as closings within a burst, and all closed intervals longer than the criterion are defined as closings between bursts. The burst criterion was set at 2.8 ms, such that the number of closings from the slower distribution falsely classified as coming from the fast

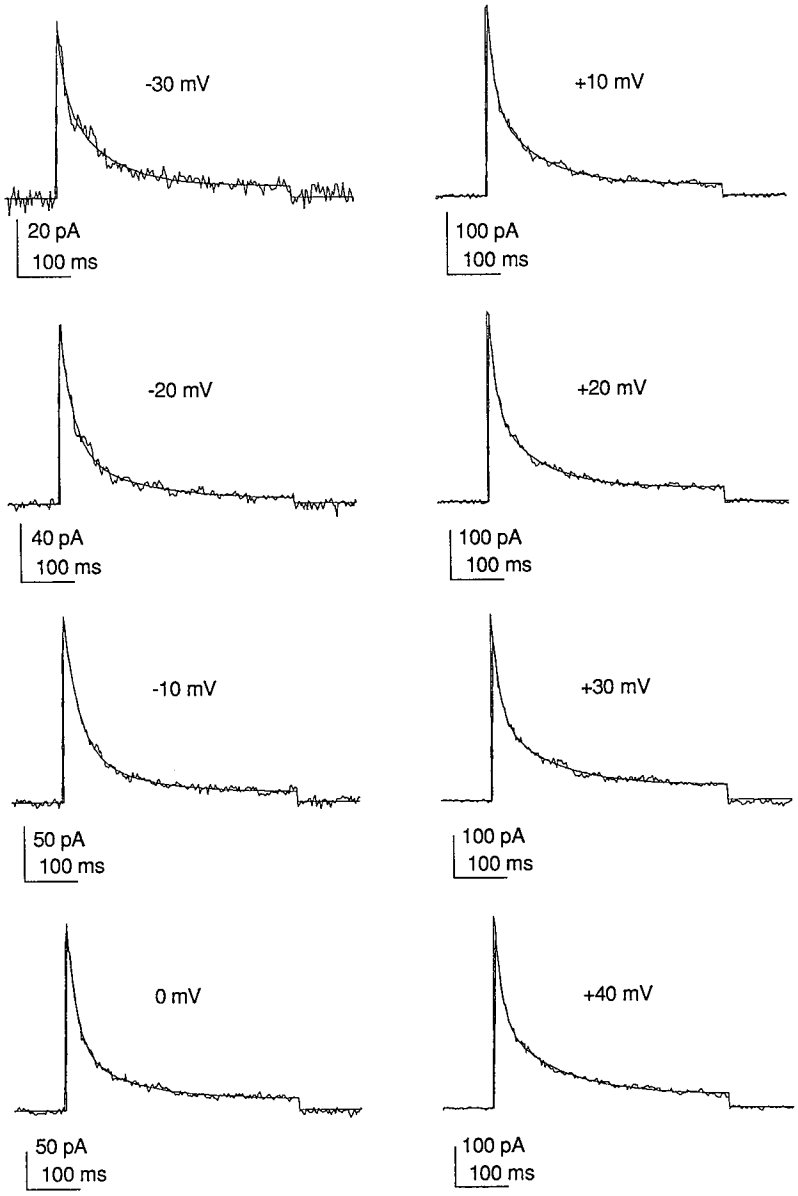

FIGURE 2. Double-exponential fits to whole-cell A currents. Same cell as in Fig. 1, *A* and *B*. The macroscopic inactivation time course of whole-cell A currents recorded at voltages between −30 and +40 mV was fitted with a sum of two exponentials. Data points between just after the peak of the current (3–6 ms after depolarization) and the end of the pulse were fitted using an unweighted unconstrained least-squares error minimization routine. Prepulse voltage was −90 mV; repetition interval was 3 s. The data were filtered at 2 kHz and digitized at 3 ms per point.

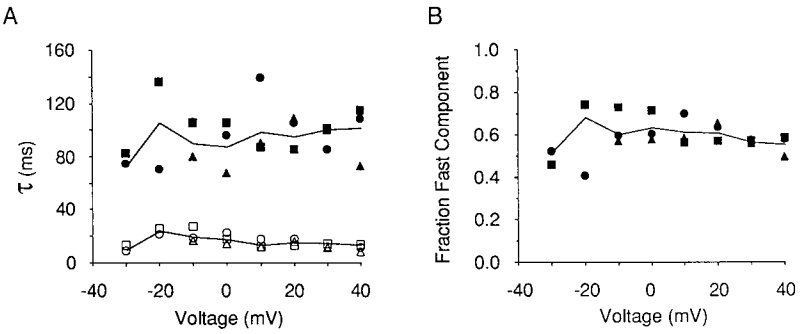

FIGURE 3. Voltage dependence of whole-cell fit time constants. (*A*) Time constants of double-exponential fits to whole-cell currents are plotted *vs.* the command voltage. The different symbols represent data from fits to three current records from the same cell. Time constants of fits to the family shown in Fig. 2 are indicated by squares. Time constants of fits to averages of two (−30, −20 mV) or three (−10 to +40 mV) current records are indicated by the lines. The two lowest voltages from one of the runs (triangles) were not fitted due to noise artifacts. (*B*) The relative amplitude of the fast component of the double-exponential fits plotted *vs.* the command voltage. The relative amplitude of the fast component from fits to the family shown in Fig. 2 is indicated by squares. The relative amplitude of the fast component from fits to averages of the currents is indicated by the line.

distribution was roughly equal to the number of closings from the fast distribution falsely classified as coming from the slower distribution (Magleby and Pallotta, 1983).

Using the burst criterion, we generated a number of duration distributions and frequency histograms with data obtained from the channel shown in Fig. 4. Distributions of first latencies, open durations, burst durations, closed durations

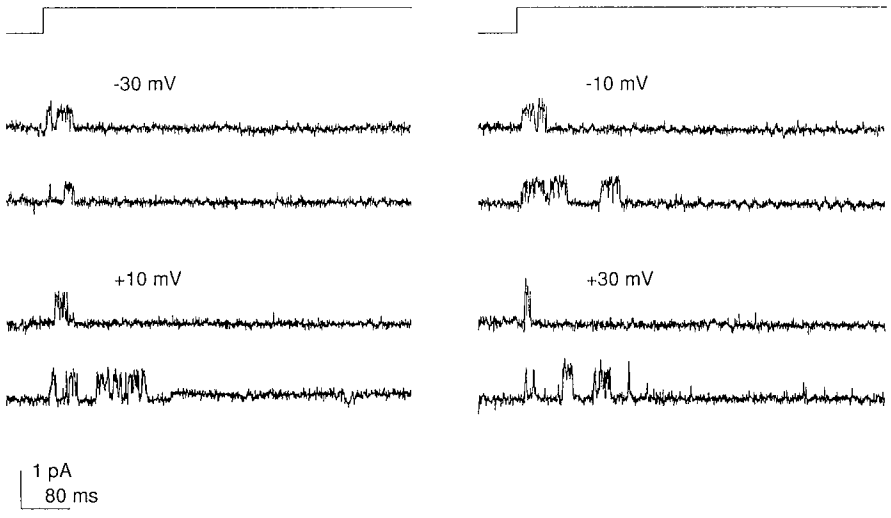

FIGURE 4. Single-channel currents from an A_2 channel in an outside-out patch recorded at −30, −10, +10, and +30 mV. The onset of the voltage pulse is indicated above the sets of records. The data were filtered at 1 kHz and digitized at 400 μs per point.

within a burst, as well as the number of openings per burst and number of bursts per trace were analyzed to provide informatioin about the nature and voltage dependence of the underlying gating transitions. The remainder of this article discusses how the above distributions, single-channel ensemble averages, and macroscopic gating properties were used to formulate and test a kinetic model of A_2 gating.

A Kinetic Model of A_2 Gating

In this section we determine the minimum number of closed, open, and inactivated states that can account for the gating properties of the A_2 channels at depolarized voltages, and arrange these states in a simple kinetic scheme. In developing this model, we did not attempt to account for channel properties at hyperpolarized voltages, such as recovery from inactivation or the prepulse inactivation curve. We have assumed that A_2 channel gating can be described by a time-homogeneous Markov process (Colquhoun and Hawkes, 1977), and have no assumptions about molecular mechanisms underlying gating. The frequency histograms discussed below are shown later in Figs. 9–12, superimposed with model-generated fits.

Open states. Open duration histograms were usually well fitted with a single exponential function. The mean open durations, however, were often longer than the fitted time constants owing to a few extraordinarily long openings. The longer openings were not resolved as a separate component, except in a few cases of channels with very slow macroscopic inactivation, and were therefore not considered in the model. All gating schemes evaluated here assumed the existence of the single open state.

Closed states. The minimum number of closed states in the opening pathway can be determined by examining the first latency distributions and the rising phase of the ensemble averages. Both of these distributions, as well as whole-cell currents, show a delay before increasing to the maxima (see Figs. 1 *C* and 5, and insets in Figs. 9–12), indicating that at least two closed states are traversed before initial opening. At least one additional (third) closed state is required to provide adequate quantitative fits to the ensemble averages and first latency distributions.

Inactivated states. Because the mean closed times between bursts are long (20–50 ms) compared with the median times to first opening (2–6 ms), the long-lifetime (interburst) closed state was not traversed in the opening pathway, and could be defined as an inactivated state. The presence of multiple bursts during a voltage step, however, indicates that channels can reenter a burst from this inactivated state, and that an additional, absorbing, inactivated state is required to account for the complete inactivation of A_2 channels observed during sufficiently long voltage steps or after depolarizing prepulses (Fig. 1 *B*).

Burst configuration. A burst could, in principle, be terminated by a transition to the nonabsorbing inactivated state either from the open state (Scheme I), or from the short-lifetime (burst) closed state (Scheme II):

$$\ldots \mathbf{C} \rightleftarrows \mathbf{O} \rightarrow \mathbf{I}$$

Scheme I

$$\ldots \mathbf{O} \rightleftarrows \mathbf{C} \rightarrow \mathbf{I}$$

Scheme II

Analysis of open, closed, and burst-related distributions alone cannot distinguish between the two schemes (Colquhoun and Hawkes, 1981; Sakmann and Trube, 1984). The following observations, however, favor the adoption of Scheme I: if the burst closed state in Scheme II is situated outside of the initial opening sequence (indicated by the dots), then the model gains an additional closed state. The quality of fits to the data, however, is no better than that obtained using Scheme I. Since Scheme I can fit the data equally well and has fewer states, it is clearly preferable. Alternatively, the burst closed state in Scheme II could be incorporated into the initial opening sequence, such that inactivation of the channels would occur only through the burst closed state (Scheme III).

$$\begin{array}{l} \ldots \mathbf{C} \rightleftarrows \mathbf{O} \\ \quad \downarrow \\ \quad \mathbf{I} \end{array}$$

Scheme III

Scheme III can provide fits to the frequency histograms equivalent to those obtainable from Scheme I. Using the rate constants required for an optimal fit to the frequency histograms, however, Scheme III is incompatible with ensemble average data. Because it allows a transition directly from the closed to the inactivated state without first going through the open state, it predicts a lower peak open probability of ensemble average currents than was observed.

A minimal kinetic model. Scheme IV is a minimal state diagram that incorporates the aspects of gating described thus far.

$$\mathbf{C}_0 \underset{\beta_0}{\overset{\alpha_0}{\rightleftarrows}} \mathbf{C}_1 \underset{\beta_1}{\overset{\alpha_1}{\rightleftarrows}} \boxed{\mathbf{C}_2 \underset{\beta_2}{\overset{\alpha_2}{\rightleftarrows}} \mathbf{O}} \underset{\beta_3}{\overset{\alpha_3}{\rightleftarrows}} \mathbf{I}_0 \underset{\beta_4}{\overset{\alpha_4}{\rightleftarrows}} \mathbf{I}_1$$

Scheme IV

Qualitatively, the scheme works as follows: At the resting membrane potential, the channel occupies state C_0. Upon depolarization, rate constants α_0 and α_1 increase and the channel enters the first burst, outlined in the diagram. The burst is a series of rapid transitions between C_2 and O, and is terminated by a transition to I_0. Once in I_0, the channel can either reenter state O and initiate another burst, or it can inactivate to I_1. Eventually, all channels end up in I_1.

A qualitative prediction of Scheme IV is that the time constant characterizing the burst closed durations cannot be slower than the rate of rise of the first latency distributions. Fig. 5 shows normalized first latency tail distributions and burst closed duration distributions superimposed at four voltages. The normalized first latency tail distributions show the probability that the delay to first opening from the onset of the depolarizing pulse was longer than the time on the abscissa, given that the channel opened during the pulse. Similarly, the burst closed duration distributions

show the probability that a closed duration was longer than the time on the abscissa. In each case, the rate of decay of the burst closed distribution is faster than the rate of decay of the first latency distribution, consistent with the idea that burst closings are to states in the opening pathway.

Another prediction of Scheme IV is that the burst duration distribution composed of only the first bursts from all the records at a particular voltage should be similar to the burst duration distribution composed of all subsequent bursts. Fig. 6 shows the first burst (*dotted line*) and subsequent burst (*solid line*) duration distributions at four voltages. The first and subsequent burst duration distributions are similar to each other at −30 mV (*A*), +10 mV (*B*), and +30 mV (*C*). No significant difference between the two distributions was detected using a two-tailed Kolmogorov-Smirnov test. At −10 mV, however, the distributions were significantly different ($P > 0.99$). Most of the difference can be accounted for by the larger number of very short (single opening, one or two sample points) bursts in the subsequent burst duration

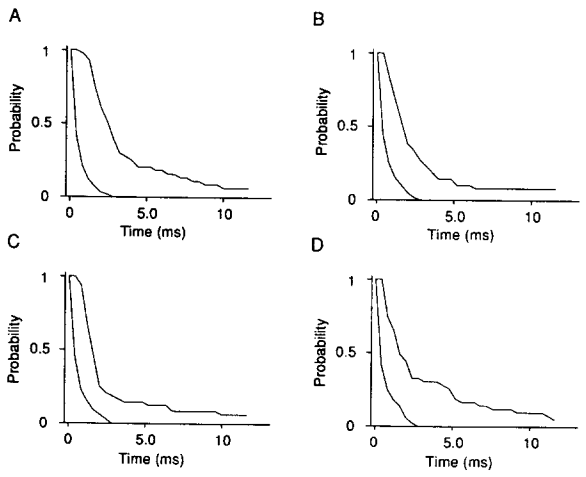

FIGURE 5. Cumulative burst closed duration distributions and first latency tail distributions at −30 (*A*), −10 (*B*), +10 (*C*), and +30 mV (*D*). The burst closed duration distributions (the rapidly decaying curve in each panel) show the probability that a closed duration within a burst was longer than the time on the abscissa. The first latency tail distributions show the probability that a first opening occurred later than the time on the abscissa, given that the channel opened at least once during the pulse.

distribution. This type of error would be expected if even a small number of random noise crossings of the 50% criterion were falsely classified as openings, because the number of noise crossings that occur in the first ~10 ms (before a channel opening) is much smaller than the number that occur in the subsequent 950 ms of the voltage step, and because the total number of events in the distributions is small enough (48 first bursts, 76 subsequent bursts) that ~10 extra short events in the subsequent burst duration distribution would be sufficient to cause the observed difference.

Fig. 7 shows a comparison of the decay time course of the ensemble averages with the burst duration distributions at four voltages. The burst duration distribution is the less noisy, more rapidly decaying trace in each panel. The cumulative burst duration distributions were scaled to the peak of the ensemble average and shifted along the abscissa by 12 ms (*A*) or 6 ms (*B–D*) to align their decay with the decay of the ensemble averages. The difference between the ensemble averages and the burst duration distributions apparent at times greater than ~20 ms after the onset of the

pulse reflects primarily channels that have re-entered a burst after an interburst closed interval, and can account for the slower component of macroscopic inactivation shown in Fig. 2.

Quantitative analysis of model. Our quantitative analysis of Scheme IV focuses on fitting transitions after the initial channel opening. This is done for two reasons: due to the small size (7 pS) and low activation voltage (−50 to −45 mV) of A_2 channels, it is difficult to obtain single-channel data of the quality necessary for modeling in the voltage range that is most interesting for activation. Furthermore, unlike NA channels (Aldrich et al., 1983) and A_1 channels (Solc et al., 1987; Zagotta et al.,

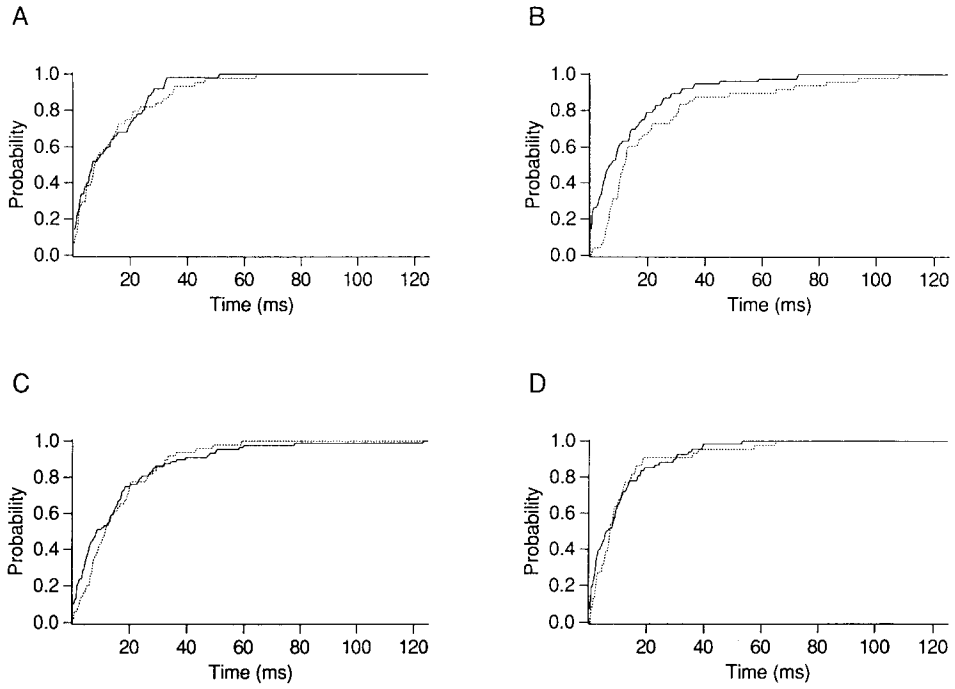

FIGURE 6. Cumulative burst duration distributions of first bursts (dotted lines) and subsequent bursts (solid lines) at −30 (*A*), −10 (*B*), +10 (*C*), and +30 mV (*D*). Burst duration distributions show the probability that a burst lasted less than or equal to the time on the abscissa.

1988; Zagotta and Aldrich, 1990), inactivation of A_2 channels is slow compared to activation, and activation rates do not contribute substantially to macroscopic inactivation. The activation process was therefore reduced to the minimum number of states necessary to fit the rising phase of the ensemble averages and to account for a delay in the first latency distributions.

Transitions among states. Because the predominant component of the burst closed duration distributions (see *D* in Figs. 9–12) is reasonably well approximated by a single exponential, transitions from C_2 back to C_1 or C_0 are unlikely. This notion is

supported by the fact that the first latency distributions have longer durations than the burst closed duration distributions (Fig. 5), and indicates that rate constants β_0 and β_1 are small at the depolarized voltages where we have observed channel opening. If this were not the case, we would expect to see a voltage dependence in the open, closed, or burst closed duration distributions, since at least one of the backward rates must be voltage dependent. As will be shown later, this was not observed. Rate constants β_0 and β_1 were therefore set to zero for the quantitative analysis. To the extent that β_0 and β_1 cannot be approximated by zero, the shapes of the burst closed duration, burst duration, and number of openings per burst

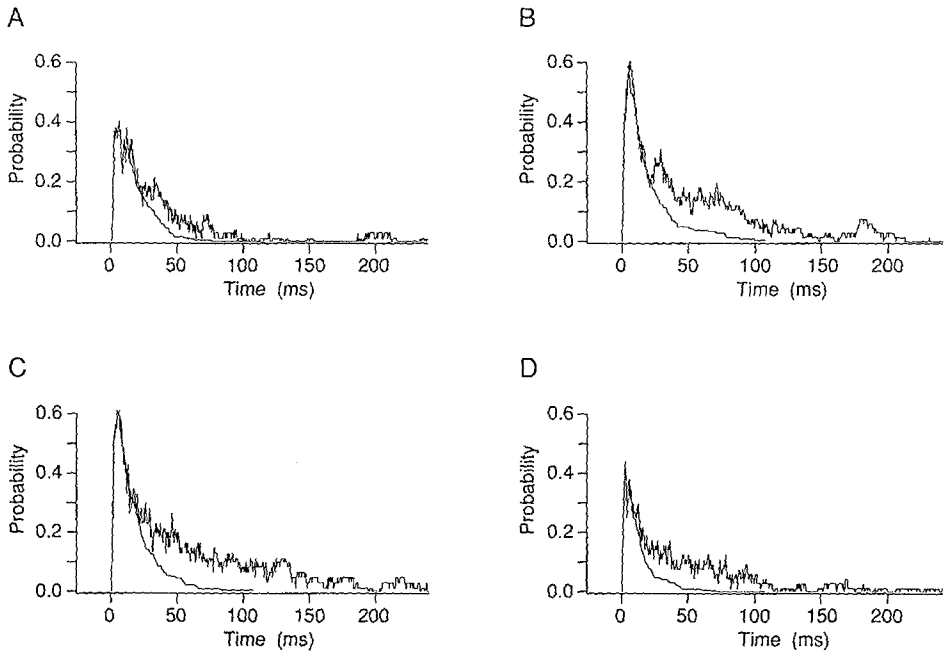

FIGURE 7. Ensemble averages of single-channel currents and cumulative burst duration distributions at −30 (*A*), −10 (*B*), +10 (*C*), and +30 mV (*D*). Burst duration distributions, normalized to the peaks of the ensemble averages, show the probability that a burst lasted longer than the time on the abscissa plus an offset of 12 (*A*) or 6 ms (*B–D*).

distributions will deviate from those derived below, but the essential kinetic behavior of the model will not be affected. Rate constant β_4 was set to zero since I_1 was defined as an absorbing state, and because the probability of steady-state openings is extremely low.

Closed state inactivation. 25–50% of the records from single A_2 channel patches had no openings. This could be because the openings were missed owing to limited sampling frequency, because the channels had not fully recovered from inactivation at the time of the depolarizing pulse, or because a path existed directly from the

closed to the inactivated states. Because A_2 channels opened, on average, several times during a depolarizing epoch, the percentage of apparently blank traces in which a channel had actually opened but was missed due to limited sampling frequency was estimated to be very small (<0.01%). The rate of recovery from inactivated states was measured in the whole-cell configuration using a double-pulse experiment. Two depolarizing pulses, separated by a −100-mV interpulse interval of varying duration, were applied at 5-s intervals. The recorded current traces in Fig. 8 *A* show recovery of the current with increasing interpulse interval durations. Fig. 8 *B* shows the relative amplitude of the current elicited by the second depolarizing pulse as a function of the interpulse interval. The symbols represent an average of three consecutive runs. The current recovery was fitted with a single

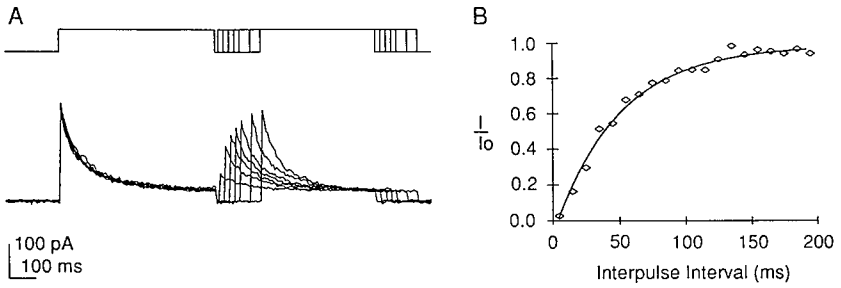

FIGURE 8. Recovery from inactivation of whole-cell A current. (*A*) The cell membrane was depolarized from a prepulse voltage of −100 mV to a command voltage of +20 mV, repolarized to −100 mV for a variable interval, and depolarized again to the +20 mV command voltage. The pulse protocol, shown in the top part of the panel, was applied at 5-s intervals. A currents elicited by the two-pulse protocol are shown in the bottom part of the panel. Currents elicited by the firsts pulse were of similar size from trial to trial while the currents elicited by the second pulse increased in amplitude with increasing interpulse intervals. (*B*) Peak current amplitude during the second pulse was normalized by the peak current amplitude during the first pulse for each trial and plotted against the interpulse interval. Three trials at each interpulse interval were averaged. The average values are plotted as diamonds and are fitted with a single exponential function with a time constant of 48 ms and a final value of 1.0

exponential function (time constant = 48 ms). Recovery time constants at −100 mV ranged from 38 to 55 ms, n = five cells.

A variation of this experiment was performed during virtually every whole-cell experiment, by noting whether successive depolarizations to the same potential, separated by the standard 3- or 5-s interpulse interval, elicit comparable-sized currents. With the exception of a relatively slow run-down process (tens of minutes), the currents were of similar size. Because in single-channel experiments the interpulse and prepulse intervals were long (5 s, 500 ms, respectively) compared with the recovery time course, the blank sweeps are likely due to inactivation from closed state(s) and not from a failure to recover. Though we have no data to exclude other

transitions, for the purpose of analysis, we represent closed state inactivation only by a transition from C_1 to I_1.

Scheme V shows the working model with the permitted transitions indicated by arrows.

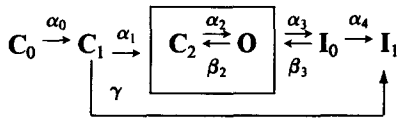

Scheme V

Equations predicted by model. Equations for the distributions and the means of the distributions predicted by Scheme V are described below. The equations for open, burst closed, and burst durations are in the form of probability density functions (pdfs). To superimpose the pdfs directly on the duration frequency histograms, the pdfs were normalized by the bin size and the total number of events in each histogram, and displayed in units of number of events per bin width (Colquhoun and Sigworth, 1983). The equations for number of openings per burst and number of bursts per trace are in the form of geometric distributions, which were also normalized by the total number of events. A geometric distribution is characterized by q, the probability of making a transition to I_0 (openings per burst) or to I_1 (bursts per trace). The mean of geometric distribution is equal to $1/q$. Derivations for the pdfs, geometric distributions, and the means can be found in Colquhoun and Hawkes (1981) and Colquhoun and Sigworth (1983).

$$\text{pdf}_{\text{open duration}} = (\alpha_3 + \beta_2)e^{-(\alpha_3+\beta_2)t} \tag{2}$$

$$\text{Mean open duration} = \frac{1}{\alpha_3 + \beta_2} \tag{3}$$

$$\text{pfd}_{\text{burst closed duration}} = \alpha_2 e^{-\alpha_2 t} \tag{4}$$

$$\text{Mean burst closed duration} = \frac{1}{\alpha_2} \tag{5}$$

$$\text{pfd}_{\text{burst duration}} = \frac{\alpha_3}{(B - A)}((\alpha_2 - A)e^{-At} + (B - \alpha_2)e^{-Bt}) \tag{6}$$

$$A = \frac{\alpha_2 + \alpha_3 + \beta_2 + \sqrt{(\alpha_2 + \alpha_3 + \beta_2)^2 - 4\alpha_2\alpha_3}}{2} \tag{7A}$$

$$B = \frac{\alpha_2 + \alpha_3 + \beta_2 - \sqrt{(\alpha_2 + \alpha_3 + \beta_2)^2 - 4\alpha_2\alpha_3}}{2} \tag{7B}$$

$$\text{Mean burst duration} = \frac{1}{\alpha_3}\left(1 + \frac{\beta_2}{\alpha_2}\right) \tag{8}$$

$$\text{Number of openings per burst} = q(1 - q)^{n-1} \qquad n = 1, 2, 3, \ldots \tag{9}$$

$$q = \frac{\alpha_3}{\alpha_3 + \beta_2} \tag{10}$$

$$\text{Number of bursts per trace} = q(1 - q)^{n-1} \qquad n = 1, 2, 3, \ldots \tag{11}$$

$$q = \frac{\alpha_4}{\alpha_4 + \beta_3} \tag{12}$$

In addition to the above distributions, it is possible to calculate and measure the distribution of interburst intervals, a single exponential pdf with a time constant, and mean equal to the inverse of β_3. Because of the small number of events and large time intervals in this distribution, we did not fit this histogram.

The time course of the ensemble average current predicted by Scheme V was calculated numerically.

Rate constant estimation. Values of the rate constants in Scheme V can be estimated by fitting the above equations to frequency histograms of the measured distributions, or by deriving each rate in terms of the means of the relevant measured distributions. We chose the first approach in order to obtain a set of rates that provided a good fit to all the distributions, and so that we could fit the distributions rather than just use the means of those distributions. The distributions were fitted using a semiautomatic procedure involving user control, outlined as follows.

Histograms of open and burst closed durations were fitted with single-exponential probability density functions. Best fits to the open duration histograms were obtained with an unweighted least-squares optimization. The fits to the burst closed duration histograms were optimized by the method of chi-square weighted by the reciprocal of the fitting function (Colquhoun and Sigworth, 1983). Frequency histograms of burst durations were fitted with a double-exponential pdf. The determination of the quality of fit to the burst duration histograms is described below. All frequency histograms, except for burst duration histograms, were also fitted by eye to determine the fastest and slowest reasonable fits. These fits defined an acceptable range used later for modeling.

Rate constants in Scheme V were adjusted at each voltage by simultaneously monitoring the calculated (predicted) fits to the five histograms and to the ensemble average, along with the values of two error estimates. The first error estimate was a sum of squared errors between the burst duration distribution pdf generated by the model, and the measured burst duration histogram. The second error estimate was a sum of the percent errors between the means of the model-generated fits and the target fits to the remaining distributions. The target fits to the open and closed duration distributions were the means of the best-fit pdfs; target fits to the number of openings per burst and number of bursts per trace distributions were simply the means of those distributions. The rate constants were constrained so all the fits remained within the range of acceptable fits (as defined in the preceding paragraph).

The combination of rates that gave the best overall fit to the distributions and ensemble average, and low error function values was accepted as optimal.

Rate constant α_2 was set to the inverse of the best-fit time constant of the burst closed durations. The ratio of α_4 to β_3 was constrained by the number of bursts per trace, and the absolute values were adjusted to provide a good fit to the ensemble average (see below). Rate constants β_2 and α_3 were constrained by three distributions: open durations, burst durations, and number of openings per burst. The relative effect of each distribution on β_2 and α_3 is discussed later. Rate constants used to fit the histograms were used to numerically calculate the probability of being in the open state as a function of time. This was compared to the ensemble average and the fit was optimized by varing the absolute values of α_4 and β_3, activation rate constants α_0 and α_1, and γ, the rate constant from C_1 to I_1. Rate constants α_0 and α_1 were adjusted to account for the initial delay and rise time of the ensemble averages. The data are fitted equally well if the values of α_0 and α_1 are interchanged, that is, if α_0 is the slower of the two rate constants.

Fits of model to single-channel data. Ensemble averages and frequency histograms of duration distributions superimposed by fits generated using the rate constants indicated are shown in Figs. 9–12 for command voltages of -30, -10, $+10$, and $+30$ mV. In each case, panel *A* shows the state diagram with the optimal rate constants for that voltage. Panels *B–D* show frequency histograms of open duration, burst duration, and burst closed duration distributions (columns), superimposed with the pdfs for those distributions (lines; Eqs. 2, 4, and 6) predicted by the state diagram in panel *A*. Panels *E* and *F* show the frequency histograms of the number of openings per burst and number of bursts per trace (columns), superimposed by the geometric distributions (●; Eqs. 9 and 11) predicted by the state diagram in panel *A*. Panel *G* shows the ensemble average superimposed with the numerical calculation of the open probability (smooth curve). The inset shows the fit to the ensemble average during the first 12 ms of the pulse on a faster time scale.

Sensitivity ranges of rate constants. The rate constants vary in the degree to which they influence the means of the predicted distributions (Eqs. 3, 5, 8, 10, and 12). A measure of this influence is necessary to evaluate the significance of any trends (such as the voltage dependence of the rate constants) apparent in the optimal set of rate constants at each voltage, and is shown for selected rate constants in Fig. 13. The rate constants used for the fits in Figs. 9–12 are indicated by filled circles, and are plotted as a function of voltage in Fig. 13, *B–F*. Shown with each rate constant are bars that represent the amount by which that rate constant must change to alter the mean of the predicted distribution (key in Fig. 13 *A*) by plus or minus 10%, given that the other rates constants that influence that distribution remain at the values indicated by the filled circles. With the exception of the burst durations, which were not independently fitted, the means of the predicted distributions used to generate the bars were set to the means of the (target) best fits to the measured distributions. Therefore, two versions of a predicted distribution, one calculated with the rate constant set to the value indicated by the top of the bar and the other calculated with the rate constant set to the value indicated by the bottom of the bar, would have means plus and minus 10% of the mean of the best fit to the measured distribution.

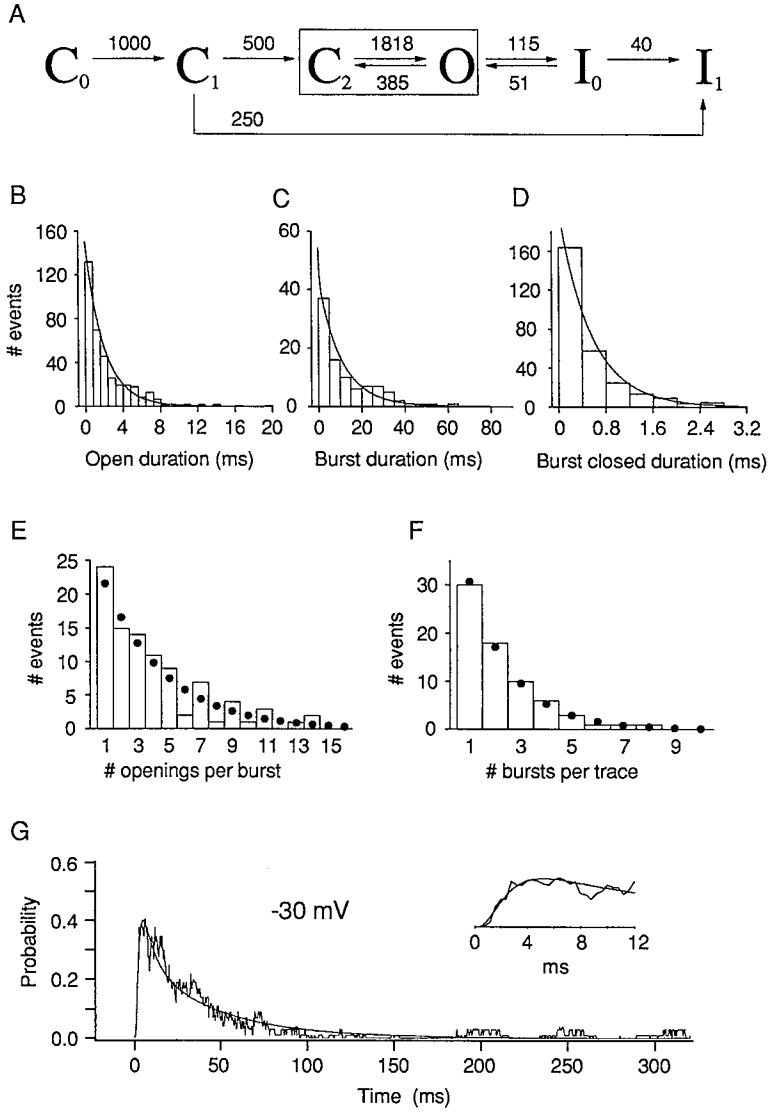

FIGURE 9. Fits of scheme V to duration distributions and ensemble average from the single-channel in Fig. 4 at −30 mV. (*A*) Model state diagram with the rate constants used to fit the distributions. (*B*) Frequency histogram of open durations shown as columns superimposed with the open duration pdf (Eq. 2). Bin size is 800 μs, $\tau = 2.0$ ms. (*C*) Frequency histogram of burst durations shown as columns superimposed with the burst duration pdf (Eq. 6). Bin size is 5 ms, $\tau_{fast} = 0.45$ ms, $\tau_{slow} = 10.64$ ms, predicted mean burst duration = 10.54 ms. (*D*) Frequency histogram of closed durations within a burst shown as columns superimposed with the burst closed duration pdf (Eq. 4). Bin size is 400 μs, $\tau = 0.55$ ms. (*E*) Frequency histogram of the number of openings per burst shown as columns superimposed with a geometric density function (Eq. 10, $q = 0.23$) shown by dots. (*F*) Frequency histogram of the number of bursts per trace, given there was at least one burst, superimposed with a geometric density function (Eq. 12, $q = 0.44$) shown by dots. (*G*) Ensemble average of 64 records superimposed with a numerical solution for open state occupancy in the state diagram in *A*. The inset shows the fit to the ensemble averages on a faster time scale.

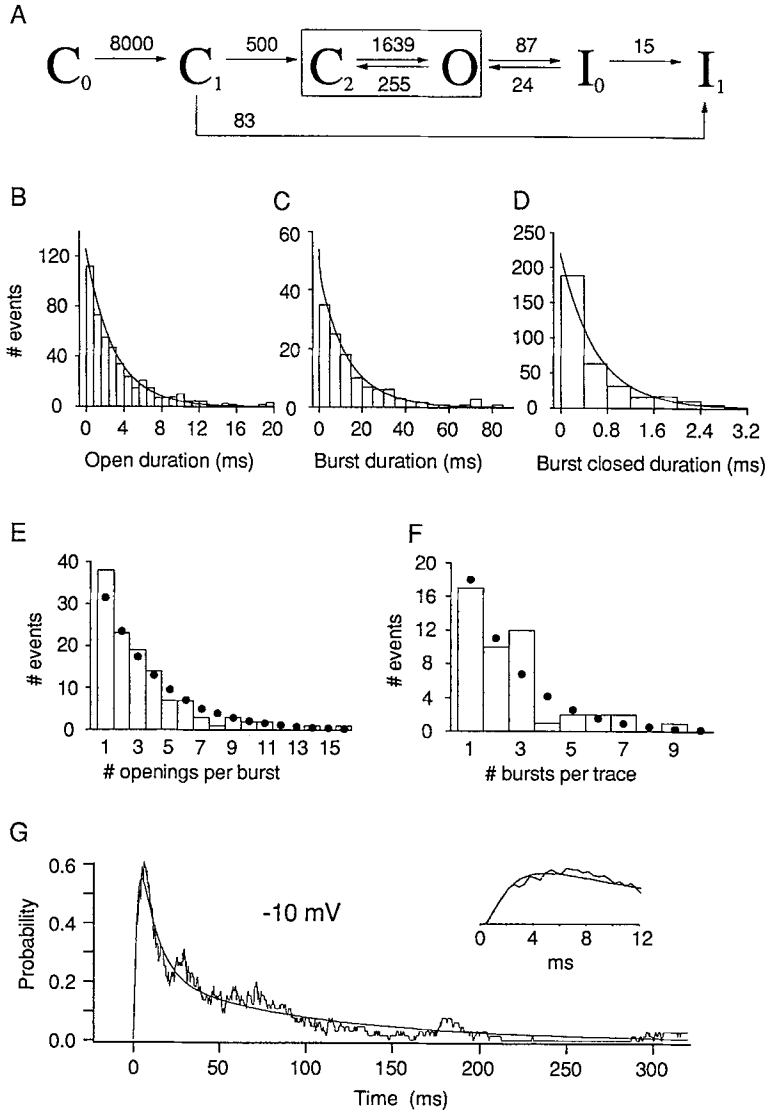

FIGURE 10. Fits of scheme V to duration distributions and ensemble average from the single-channel in Fig. 4 at −10 mV. *A–G* are analogous to those described in Fig. 9. The data and fit parameters are as follows: (*B*) bin size is 800 μs, τ = 2.92 ms; (*C*) bin size is 5 ms, τ_{fast} = 0.52 ms, τ_{slow} = 13.37 ms, predicted mean burst duration = 13.28 ms; (*D*) bin size is 400 μs, τ = 0.61 ms; (*E*) q = 0.25; (*F*) q = 0.38.

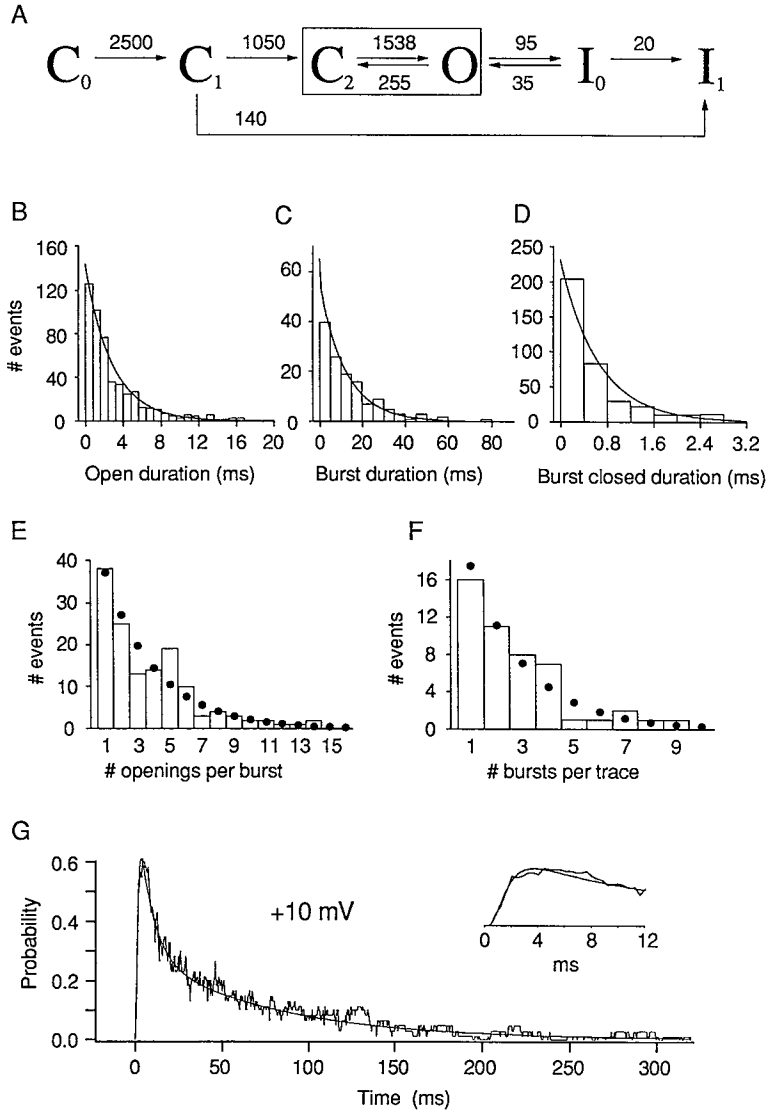

FIGURE 11. Fits of scheme V to duration distributions and ensemble average from the single-channel in Fig. 4 at +10 mV. *A–G* are analogous to those described in Fig. 9. (*B*) Bin size is 800 μs, τ = 2.86 ms. (*C*) Bin size is 5 ms, τ_{fast} = 0.55 ms, τ_{slow} = 12.37 ms, predicted mean burst duration = 12.27 ms. (*D*) Bin size is 400 μs, τ = 0.65 ms. (*E*) q = 0.27. (*F*) q = 0.36.

For the open duration and number of openings per burst distributions, the values of the rate constants that would make the predicted means equal to the best-fit means are indicated by horizontal lines in the bars. Since the optimal set of rate constants (indicated by the filled circles) was determined by taking into account fits to all the

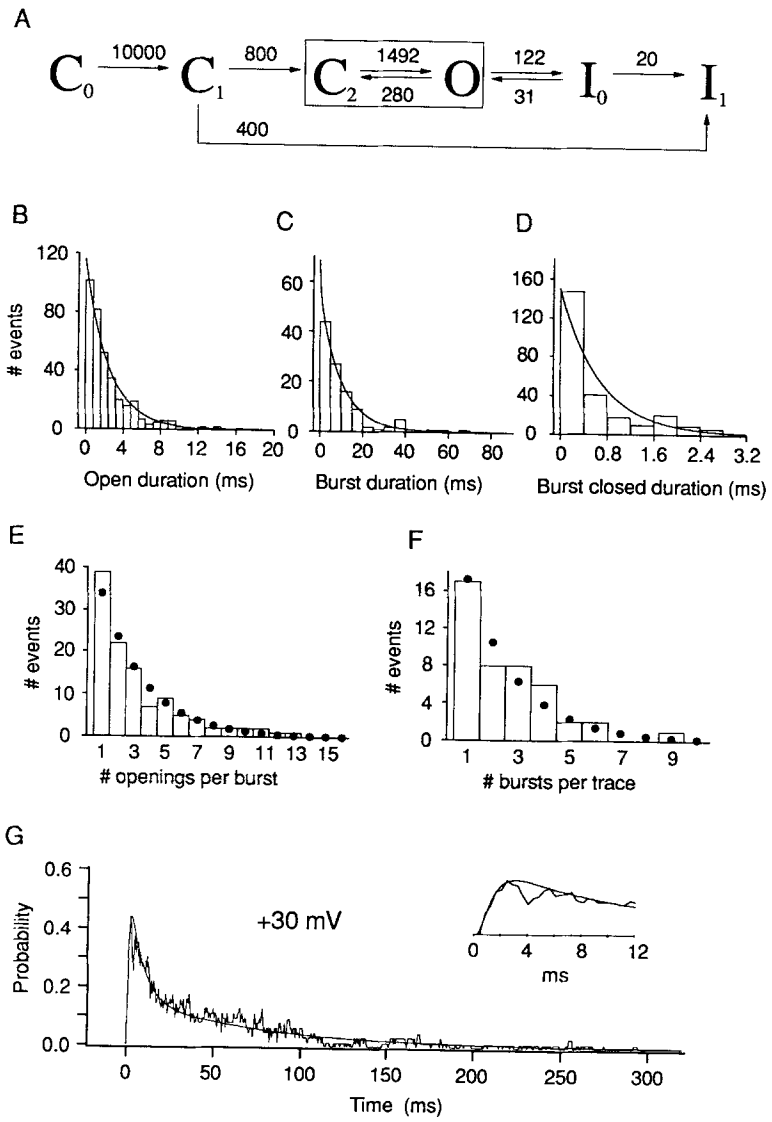

FIGURE 12. Fits of scheme V to duration distributions and ensemble average from the single-channel in Fig. 4 at +30 mV. *A–G* are analogous to those described in Fig. 9. (*B*) Bin size is 800 μs, τ = 2.49 ms. (*C*) Bin size is 5 ms, τ_{fast} = 0.56 ms, τ_{slow} = 9.85 ms, predicted mean burst duration = 9.47 ms. (*D*) Bin size is 400 μs, τ = 0.67 ms. (*E*) q = 0.30. (*F*) q = 0.39.

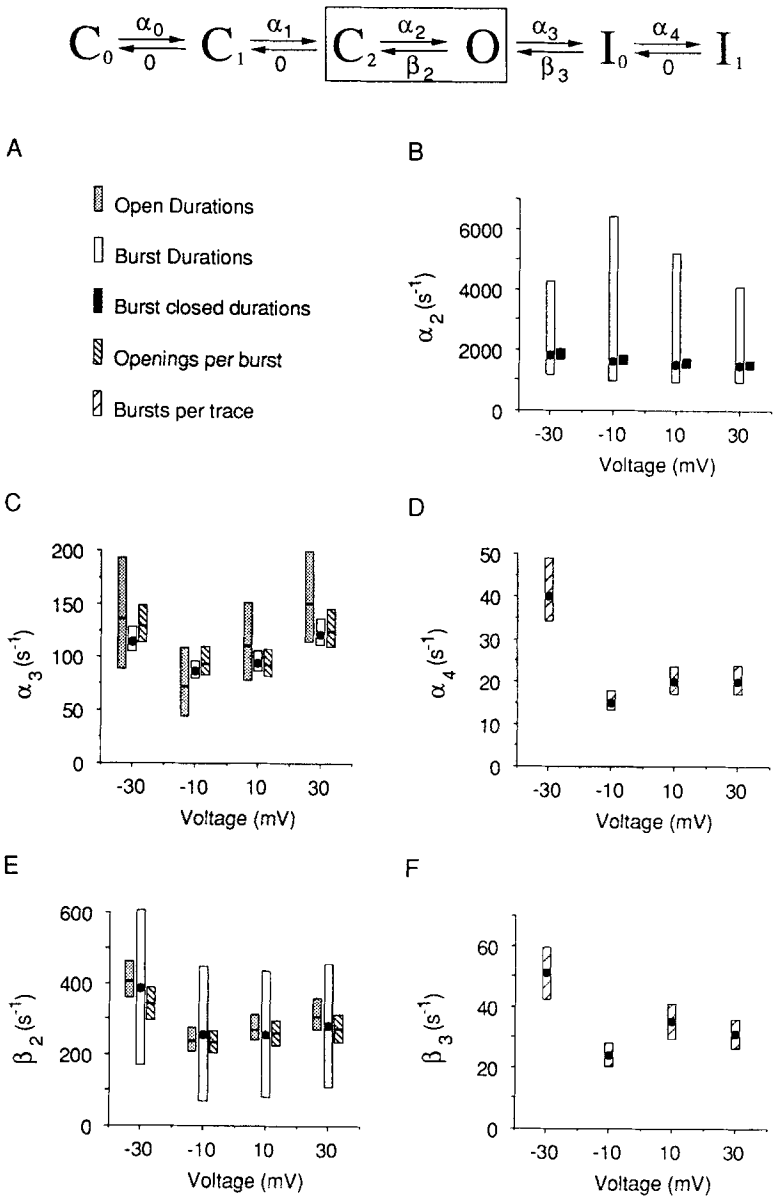

FIGURE 13. Sensitivity of predicted distribution means to the rate constants, and voltage dependence of the rate constants. The rate constants used for the fits in Figs. 9–12 are indicated by dots, and are plotted as a function of voltage in *B–F*. Along with the rate constants are bars that represent the amount by which that particular rate constant must change to alter the mean of a predicted distribution (*A*) by ± 10%, given that all other rates constants remain at the values indicated by the dots. With the exception of the burst durations, which were not independently fitted, the means of the predicted distributions used to generate the bars were set to the means of the best fits to those distributions. (*A*) Key to the symbols for the distribution ranges. (*B*) α_2 *vs.* voltage. α_2 affects burst durations and within-burst closed durations. (*C*) α_3 *vs.* voltage. α_3 affects open durations, burst durations, and the number of openings per burst. (*D*) α_4 *vs.* voltage. α_4 affects the number of bursts per trace. (*E*) β_2 *vs.* voltage. β_2 affects the open durations, burst durations, and the number of openings per burst. (*F*) β_3 *vs.* voltage. β_3 affects the number of bursts per trace.

distributions and the ensemble average, their values do not coincide exactly with those indicated by the horizontal lines. For the burst closed and number of bursts per trace distributions, the optimal rate constants are such that the predicted means are equal to the best fit means.

The longer the bars for a particular distribution, the less sensitive it is to changes in that rate constant. Fig. 13 *B* shows that the burst duration distribution is very insensitive to variations in α_2, whereas the burst closed duration distribution, which was used to determine α_2, is much more sensitive. Rate constants α_3 and β_2 make an interesting comparison. Both rate constants were determined from simultaneous fits to three distributions (open durations, burst durations, and number of openings per burst), but were not influenced by the distributions equally. The fit to the burst duration histograms was the more sensitive factor in determining α_3, whereas the fit to the open duration histogram was the more sensitive factor in determining β_2. Rate constants α_4 and β_3 are closely related. The ratio of α_4 to β_3 was constrained by the number of openings per burst, while the magnitudes of the rate constants were estimated from fits to the ensemble average. Since we did not define a parameter to reflect the range of acceptable fits to the ensemble averages, we did not include a bar that shows the influence of α_4 and β_3 on those fits.

Voltage dependence of rate constants and distributions. Inspection of the macroscopic activation kinetics of whole-cell A current, and ensemble averages and first latency distributions of A_2 channels indicates that at least some of the rate constants in the initial opening pathway are voltage-dependent. For reasons previously indicated, it was not our objective to evaluate the voltage dependence of these rate constants, but rather to investigate whether other rate constants, which we can estimate with better confidence, show a consistent and significant amount of voltage dependence. Rate constant α_2, shown in *B* of Fig. 13, decreases monotonically with voltage between -30 and $+30$ mV. This voltage dependence is opposite of that generally expected for opening rate constants of voltage-activated channels (Hodgkin and Huxley, 1952), and may be due to an increased number of false (noise-induced) closings detected at low voltages due to the smaller size of the channels. The degree of voltage dependence, assuming that the rate constant depends exponentially on voltage (Stevens, 1978), is very small (*e*-fold for ~300 mV). Rate constants α_3, α_4, β_2, and β_3 do not show a consistent trend with voltage.

The lack of a relationship between the rate constants and voltage could in principle be due to a bias in the fitting procedure, so we compared the voltage dependence of the means of measured distributions with the voltage dependence of the means of the distributions predicted by the model. These data are shown in Fig. 14. Like the rate constants in Fig. 13, the means of the measured distributions do not show a consistent voltage dependence. Furthermore, with the exception of the burst duration distributions (which were not independently fitted), the distribution means predicted by the model generally agree well with the best-fit means of the measured distributions.

Taken together, the above results suggest that transition rates after initial opening are not very voltage-dependent.

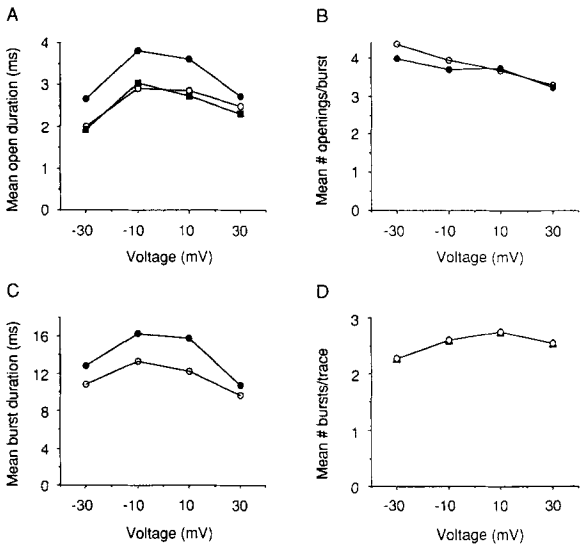

FIGURE 14. Voltage dependence of the means of measured and predicted distributions. Filled symbols represent the means of the measured distributions; open symbols represent the means of the distributions predicted by the model. (*A*) Open duration distributions. (●) Mean open durations; (■) means of the best fits to the histograms; (○) means of the open duration distributions predicted by the model. (*B*) Number of openings per burst. (●) Mean number of openings per burst and open circles represent mean number of openings per burst predicted by the model. (*C*) Burst duration distributions. (●) Mean burst duration distributions; (○) means of the burst durations predicted by the model. (*D*) Number of bursts per trace. (▲) Measured mean number of bursts per trace; (○) mean number of bursts per trace predicted by the model.

Variation of parameters between experiments. The single-channel data shown thus far were obtained from one experiment (no. 186) on a single A_2 channel. A_2 channels were observed in 56 patches. Of those, 12 were suitable for detailed analysis based on the signal to noise ratio, the relative absence of other channels, and lifetime and stability of the patch. Of the 12 patches analyzed in detail, five had only a single channel. Of the five, only one patch (no. 186) remained stable long enough to gather data at several voltages. Data from another of the single-channel patches (no. 392), from a *Shaker*-deficient fly, were also fitted. The fact that the macroscopic kinetic parameters of the ensemble average currents from patch 186 closely resemble the kinetic properties of whole-cell currents, and that virtually all of the ensemble averages of A_2 channels from other patches ($n = 12$) decayed with a double-exponential time course suggests that the kinetic properties of this channel are representative of A_2 channels in general. Model-independent parameters from the three other single-channel patches, in addition to nos. 186 and 392, are shown in Table I.

Fits of model to whole-cell data. Scheme V, using rates like those in Figs. 9–12, predicts a double-exponential macroscopic inactivation time course. If the channel used in the analysis is representative, the magnitude and proportion of the time constants in the predicted current inactivation should be similar to those observed in fits to whole-cell inactivation. The open state probability time course predicted by the model was fitted with a sum of two exponentials and a baseline using the same algorithm used to fit the whole-cell currents in Fig. 2. The double exponential fit in each case was indistinguishable from the model-generated curve. Parameters of these

TABLE I

Model-independent Parameters from Single-Channel Patches

Parameter	Patch No.				
	173	186	225	344	392
Mean open duration	3.30	2.73	4.01	5.94	2.50
Peak open probability	0.69	0.44	0.54	0.59	0.51
Mean burst duration	16.7	10.7	15.3	46.7	9.4
Number of openings per burst	4.30	3.24	3.36	7.10	3.12
Number of bursts per trace	2.18	2.55	2.07	2.25	3.19

fits are compared in Fig. 15 to the parameters of fits to the average currents in Fig. 2. Although the single-channel fits in this particular instance are slightly faster than the whole-cell fits, there is good correspondence in the relative size of the time constants, and in the proportions with which they are expressed. The significance of the discrepancy in the fits is minimized in light of the statistical variation inherent in examining a single channel from a large population, and by the scatter apparent in consecutive fits to currents from a single cell (Fig. 2).

A_2 Channels from Shaker Deficiency Flies

In an earlier report, we showed that that the A_2 channels in larval *Drosophila* neuron cell-bodies are distinct from the *Shaker* A_1 channels found in *Drosophila* muscle, and that the A_2 channels are present in flies homozygous for the Sh^{KS133} and Sh^5 mutations. These results, along with the differences in single-channel properties, were used to suggest that A_2 channels are coded for by a gene other than *Shaker*. Subsequent cloning of *Shaker* has revealed the presence of many different mRNAs formed by differential splicing (Baumann et al., 1987; Kamb et al., 1987, 1988; Papazian et al., 1987; Tempel et al., 1987; Pongs et al., 1988; Schwarz et al., 1988).

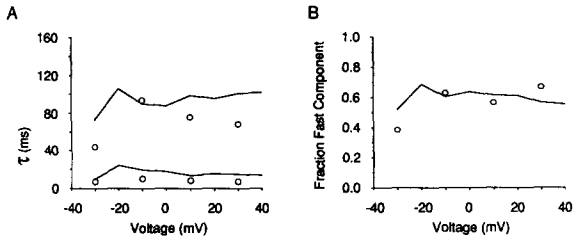

FIGURE 15. Fits to inactivation of ensemble averages compared to fits of whole-cell current. (*A*) Time constants of a double-exponential fit to the open state probability, calculated at each voltage using the rate constants in Figs. 9–12 are represented as open circles. Time constants of fits to averaged whole-cell currents (from Fig. 3) are represented as lines. (*B*) The relative amplitude of the fast component of the double-exponential fits plotted *vs.* the command voltage. The relative amplitude of the fast component from fits to the calculated open probability is indicated by open circles. The relative amplitude of the fast component from fits to the whole-cell current averages is indicated by the line.

At least some of these RNA species can code for functional potassium channels in *Xenopus* oocytes that can be distinguished on the basis of their gating properties (Iverson et al., 1988; Timpe et al., 1988*a*, *b*). Since the lack of an effect of *Shaker* on A_2 channels in our previous report was based on the analysis of only two mutations, we performed experiments to test if any part of the *Shaker* locus alters the gating of A_2 channels. Single A_2 channels recorded from flies with a deficiency that deletes most of the *Shaker* coding region (Papazian et al., 1987) are shown in Fig. 16. The channels are indistinguishable from A_2 channels from wild-type flies. Data from the channel illustrated in Fig. 16 were analyzed in the same way as the data from the channel in Fig. 4. Measured histograms superimposed with the predicted fits (panels

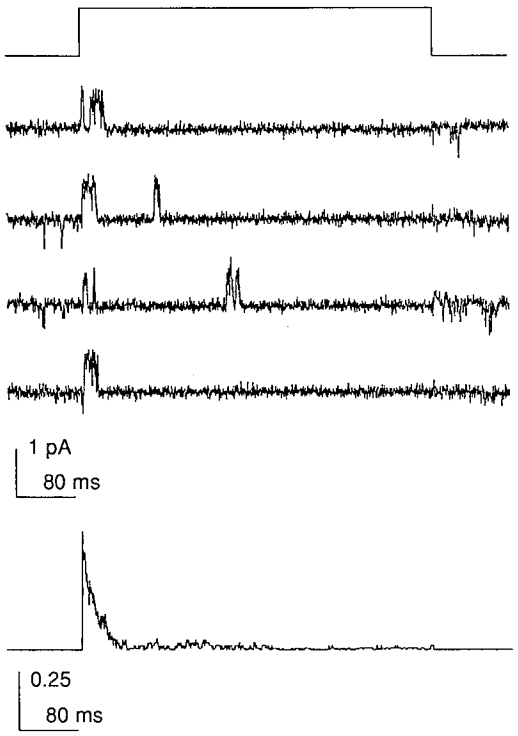

FIGURE 16. Single A_2 channel currents and ensemble averages from flies homozygous for a deficiency at the *Shaker* locus. Single-channel currents, shown in the top panel, were evoked by steps to +30 mV from a prepulse voltage of −120 mV. The lower panel shows the ensemble average current. The data were filtered at 1 kHz, digitized at 400 μs per point, and digitally filtered at 750 Hz.

B–F), and the ensemble average superimposed by the calculated *P(O)* (panel *G*) are shown in Fig. 17. The optimal rate constants are similar to those for wild-type flies.

DISCUSSION

We have analyzed the whole-cell and single-channel gating properties of A_2 channels and have proposed a kinetic model that can account for their gating.

Several assumptions were made in formulating the kinetic model. One assumption was that rate constants β_0 and β_1 could be approximated by zero. If this assumption is not true, the conclusions from the model would remain essentially unchanged, but

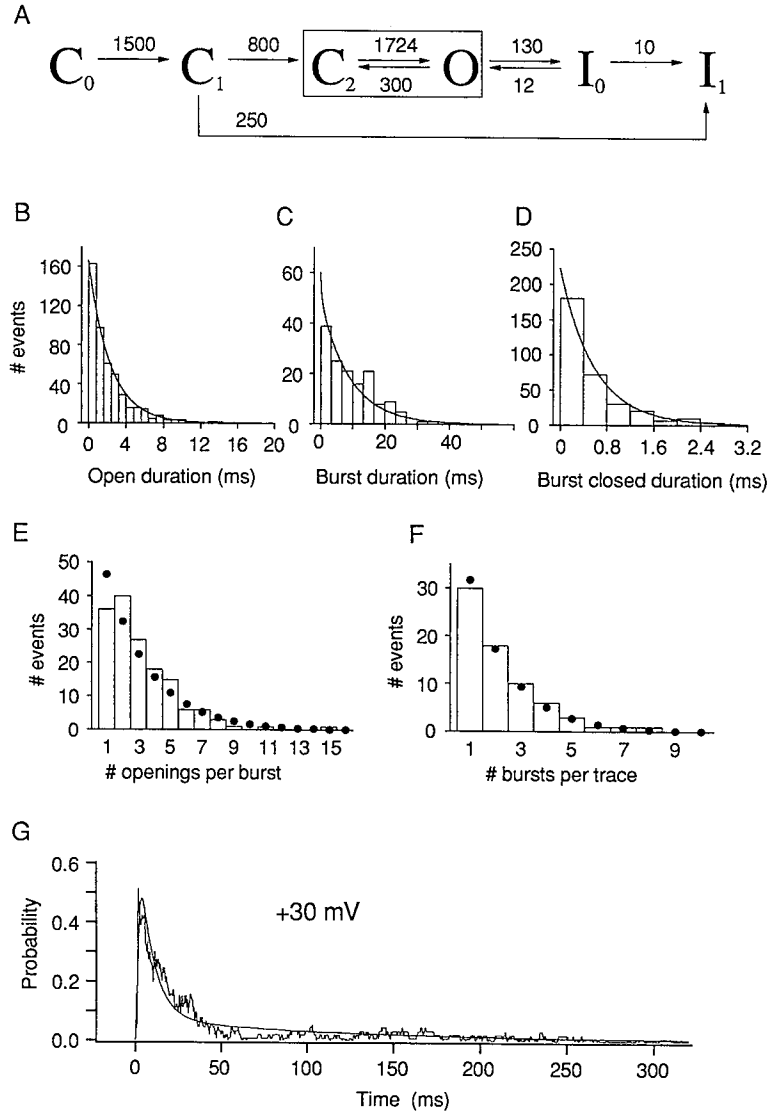

FIGURE 17. Fits of scheme V to duration distributions and ensemble average from the single A_2 channel in Fig. 16. *A–G* are analogous to those described in Fig. 8. (*B*) Bin size is 800 μs, τ = 2.33 ms. (*C*) Bin size is 3.3 ms, τ_{fast} = 0.49 ms, τ_{slow} = 9.12 ms, predicted mean burst duration = 9.03 ms. (*D*) Bin size is 400 μs, τ = 0.58 ms. (*E*) q = 0.30. (*F*) q = 0.46.

the following effects on the distributions would be expected: if the channel can enter state C_1 during a burst but cannot inactivate from that state, and if all other rate constants remain unchanged, then a burst would on average last slightly longer than that predicted, and the burst closed duration distribution would exhibit a second component. The burst duration could be increased by decreasing β_2 and increasing

α_3 without affecting open durations, but the number of openings per burst would decrease. The effect would be reduced if the channel could inactivate from C_1 (as indicated in Scheme V).

The data were not corrected for missed events. This also does not affect the general conclusions from the model, but changes the values of some of the rates: since there is no evidence of a very fast component in the open time distributions, most of the missed events are likely to be closings rather than openings. If we were able to detect the missed closings, we would expect a decrease in the mean burst closed durations (increase in α_2), a decrease in the mean open durations (increase in β_2), and a corresponding increase in the number of openings per burst. We would not expect, however, a substantial effect on the burst durations or on the number of bursts per trace.

The model bears a strong similarity to models of other inactivating voltage-dependent channels that were developed on the basis of single-channel recording (Aldrich et al., 1983; Aldrich and Stevens, 1987; Zagotta and Aldrich, 1990). All these models are related in the arrangement of states, and in that essentially all of the voltage dependence lies in the opening pathway, such that transitions occurring after the first opening are largely independent of voltage. The voltage-dependent macroscopic inactivation in Na and A_1 channels is due to the voltage dependence of the first latency distributions. Because the open and burst durations in those channels are on the same time-scale as the first latencies, the macroscopic inactivation time course at low voltages is dominated by the relatively slow opening process (first latencies). At the higher voltages, where the channels open more rapidly, the macroscopic inactivation is limited by the open or burst durations. Burst durations of A_2 channels are long compared to the first latency distributions, so macroscopic inactivation is not strongly influenced by transitions in the opening pathway. Since transitions after first opening are also independent of voltage, the macroscopic inactivation is not voltage dependent. The differences between A_2 channels and channels with faster, more voltage-dependent, macroscopic inactivation can thus be accounted for by differences in the relative magnitudes of a few voltage-independent rate constants, most notably, the inactivation rate constants.

The presence of A_2 channels in cells from *Shaker* deficiency flies indicates that the channels are coded for by a gene other than *Shaker,* but the qualitative similarity in gating mechanisms suggests that the structure of the A_2 channel protein will have some similarities with the *Shaker* channel protein. Butler et al. (1989) have found two clones in *Drosophila, shaw* and *shab,* that have a strong homology to *Shaker.* Although it is likely that other potassium channel genes are present in the fly genome and will be isolated in the near future, it is possible that either *shaw* or *shab* is from the locus that codes for A_2 channels.

We thank Dr. Denis Baylor for helpful comments on the manuscript.

This work was supported by National Institutes of Health grant NS-23294 to Dr. Aldrich, a fellowship from the Alfred P. Sloan Foundation to Dr. Aldrich, and an NSF graduate fellowship to Dr. Solc.

Original version received 11 September 1989 and accepted version received 27 December 1989.

REFERENCES

Adams, D. J., S. J. Smith, and S. H. Thompson. 1980. Ionic currents in molluscan soma. *Annual Review of Neuroscience.* 3:141–167.

Adams, P. R., and M. Galvan. 1986. Voltage-dependent currents of vertebrate neurons and their role in membrane excitability. *Advances in Neurology.* 44:137–170.

Aldrich, R. W., D. P. Corey, and C. F. Stevens. 1983. A reinterpretation of mammalian sodium channel gating based on single-channel recording. *Nature.* 306:436–441.

Aldrich, R. W., and C. F. Stevens. 1987. Voltage-dependent gating of single sodium channels from mammalian neuroblastoma cells. *Journal of Neuroscience.* 7:418–431.

Baumann, A., I. Krah-Jentgens, R. Muller, F. Muller-Holtkamp, R. Seidel, N. Kecskemethy, J. Casal, A. Ferrus, and O. Pongs. 1987. Molecular organization of the maternal effect region of the *Shaker* complex of *Drosophila:* characterization of an IA channel transcript with homology to vertebrate Na^+ channel. *European Molecular Biology Organization Journal.* 6:3419–3429.

Butler, A., A. Wei, K. Baker, and L. Salkoff. 1989. A family of putative potassium channel genes in *Drosophila. Science.* 243:943–947.

Chiu, S. Y. 1977. Inactivation of sodium channels: second-order kinetics in myelinated nerve. *Journal of Physiology.* 273:573–596.

Colquhoun, D., and A. G. Hawkes. 1977. Relaxation and fluctuations of membrane currents that flow through drug-operated ion channels. *Proceedings of the Royal Society of London Series B Biological Sciences.* 199:231–266.

Colquhoun, D., and A. G. Hawkes. 1981. On the stochastic properties of ion channels. *Proceedings of the Royal Society of London Series B Biological Sciences.* 211:205–235.

Colquhoun, D., and F. J. Sigworth. 1983. Fitting and statistical analysis of single channel records. *In* Single Channel Recording. B. Sakmann and E. Neher, editors. Plenum Publishing Corp., New York. 191–264.

Connor, J. A., and C. F. Stevens. 1971*a*. Voltage clamp studies of a transient outward membrane current in gastropod neural somata. *Journal of Physiology.* 213:21–30.

Connor, J. A., and C. F. Stevens. 1971*b*. Prediction of repetitive behaviour from voltage clamp data on an isolated neurone soma. *Journal of Physiology.* 213:31–53.

Conti, F., and E. Neher. 1980. Single channel recordings of K^+ currents in squid axons. *Nature.* 285:140–143.

Ganetzky, B., and C.-F. Wu. 1983. Neurogenetic analysis of potassium currents in *Drosophila:* synergistic effects on neuromuscular transmission in double mutants. *Journal of Neurogenetics.* 1:17–28.

Ganetzky, B., and C.-F. Wu. 1985. Genes and membrane excitability in *Drosophila. Trends in Neurosciences.* 8:322–326.

Hagiwara, S., K. Kusano, and N. Saito. 1961. Membrane changes of *Onchidium* nerve cell in potassium-rich media. *Journal of Physiology.* 155:470–489.

Hamill, O. P., A. Marty, E. Neher, B. Sakmann, and F. J. Sigworth. 1981. Improved patch clamp techniques for high-resolution current recording from cells and cell-free membrane patches. *Pflügers Archives.* 391:85–100.

Hodgkin, A. L., and A. F. Huxley. 1952. A quantitative description of membrane current and its application to conduction and excitation in nerve. *Journal of Physiology.* 117:500–544.

Iverson, L. E., M. A. Tanouye, H. A. Lester, N. Davidson, and B. Rudy. 1988. A-type potassium channels expressed from *Shaker* locus cDNA. *Proceedings of the National Academy of Sciences.* 85:5723–5727.

Jan, Y. N., L. Y. Jan, and M. J. Dennis. 1977. Two mutations of synaptic transmission in *Drosophila*. *Proceedings of the Royal Society of London Series B Biological Sciences*. 198:87–108.

Kamb, A., L. E. Iverson, and M. A. Tanouye. 1987. Molecular characterization of *Shaker*, a *Drosophila* gene that encodes a potassium channel. *Cell*. 50:405–413.

Kamb, A., J. Tseng-Crank, and M. A. Tanouye. 1988. Multiple products of the *Drosophila Shaker* gene may contribute to potassium channel diversity. *Neuron*. 1:421–430.

Latorre, R., R. Coronado, and C. Vergara. 1984. K^+ channels gated by voltage and ions. *Annual Review of Physiology*. 46:485–495.

Magleby, K. L., and B. S. Pallotta. 1983. Burst kinetics of single calcium-activated potassium channels in cultured rat muscle. *Journal of Physiology*. 344:605–623.

Neher, E. 1971. Two fast transient current components during voltage clamp on snail neurons. *Journal of General Physiology*. 58:36–53.

Nelson, D. J., and F. Sachs. 1979. Single ionic channels observed in tissue-cultured muscle. *Nature*. 282:861–863.

Papazian, D. M., T. L. Schwarz, B. L. Tempel, Y. N. Jan, and L. Y. Jan. 1987. Cloning of genomic and complementary DNA from *Shaker*, a putative potassium channel gene from *Drosophila*. *Science*. 237:749–753.

Patlak, J. B., K. A. F. Gration, and P. N. R. Usherwood. 1979. Single glutamate-activated channels in locust muscle. *Nature*. 278:643–645.

Pongs, O., N. Kecskemethy, R. Muller, I. Kreh-Jentgens, A. Baumann, H. H. Kiltz, I. Canal, S. Llamazares, and A. Ferrus. 1988. *Shaker* encodes a family of putative potassium channel proteins in the nervous system of *Drosophila*. *European Molecular Biology Organization Journal* 7:1087–1096.

Rudy, B. 1988. Diversity and ubiquity of K^+ channels. *Neuroscience*. 25:729–750.

Sakmann, B., J. Patlak, and E. Neher. 1980. Single acetylcholine-activated channels show burst-kinetics in the presence of desensitizing concentrations of agonist. *Nature*. 286:71–73.

Sakmann, B., and G. Trube. 1984. Voltage-dependent inactivation of inward-rectifying single-channel currents in the guinea-pig heart cell membrane. *Journal of Physiology*. 347:659–683.

Salkoff, L. B., and R. Wyman. 1981*a*. Outward currents in developing *Drosophila* flight muscle. *Science*. 212:461–463.

Salkoff, L. B., and R. Wyman. 1981*b*. Genetic modification of potassium channels in *Drosophila Shaker* mutants. *Nature*. 293:228–230.

Schwarz, T. L., B. L. Tempel, D. M. Papazian, Y. N. Jan, and L. Y. Jan. 1988. Multiple potassium-channel components are produced by alternative spicing at the *Shaker* locus of *Drosophila*. *Nature*. 331:137–142.

Sigworth, F. J. 1981. Covariance of nonstationary sodium current fluctuations at the node of ranvier. *Biophysical Journal*. 34:111–133.

Solc, C. K. 1989. The gating of voltage-dependent potassium channels in CNS neurons of *Drosophila*. Ph.D. thesis. Stanford University, Stanford, CA.

Solc, C. K., and R. W. Aldrich. 1988. Voltage-gated potassium channels in larval CNS neurons of *Drosophila*. *Journal of Neuroscience*. 8:2556–2570.

Solc, C. K., W. N. Zagotta, and R. W. Aldrich. 1987. Single-channel and genetic analyses reveal two distinct A-type potassium channels in *Drosophila*. *Science*. 236:1094–1098.

Stevens, C. F. 1978. Interactions between intrinsic membrane protein and electric field. *Biophysical Journal*. 22:295–306.

Tanouye, M. A., A. Ferrus, and S. C. Fujita. 1981. Abnormal action potentials associated with the *Shaker* complex locus of *Drosophila*. *Proceedings of the National Academy of Sciences*. 78:6548–6552.

Tempel, B. L., D. M. Papazian, T. L. Schwarz, Y. N. Jan, and L. Y. Jan. 1987. Sequence of a probable potassium channel component encoded at *Shaker* locus of *Drosophila*. *Science.* 237:749–753.

Thompson, S. H., and R. W. Aldrich. 1980. Membrane potassium channels. *In* The Cell Surface and Neuronal Function. C. W. Cotman, G. Poste and G. L. Nicolson, editors. Elsevier/North Holland Biomedical Press, Amsterdam. 49–85.

Timpe, L. C., Y. N. Jan, and L. Y. Jan. 1988*a*. Four cDNA clones from the *Shaker* locus of *Drosophila* induce kinetically distinct A-type potassium currents in *Xenopus* oocytes. *Neuron.* 1:659–667.

Timpe, L. C., T. L. Schwarz, B. L. Tempel, D. M. Papazian, Y. N. Jan, and L. Y. Jan. 1988*b*. Expression of functional potassium channels from *Shaker* cDNA in *Xenopus* oocytes. *Nature.* 331:143–145.

Wu, C.-F., N. Suzuki, and M.-M. Poo. 1983. Dissociated neurons from normal and mutant *Drosophila* larval central nervous system in cell culture. *Journal of Neuroscience.* 3:1888–1899.

Zagotta, W. N., and R. W. Aldrich. 1990. Voltage-dependent gating of *Shaker* A-type potassium channels in *Drosophila* muscle. *Journal of General Physiology.* In press.

Zagotta, W. N., M. S. Brainard, and R. W. Aldrich. 1988. Single-channel analysis of four distinct classes of potassium channels in *Drosophila* muscle. *Journal of Neuroscience.* 8:4765–4779.

Zagotta, W. N., T. Hoshi, and R. W. Aldrich. 1989. Gating of single Shaker K^+ channels in *Drosophila* muscle and in *Xenopus* oocytes injected with *Shaker* mRNA. *Proceedings of the National Academy of Sciencies.* 86:7243–7247.